RSC Advances

ROYAL SOCIETY OF CHEMISTRY

www.rsc.org/advances

RSC Advances

ARTICLE

Tailored synthesis of CoO_X thin films for catalytic application

Shi-Bin Fan,[a,b] Guan-Fu Pan,[a,b] Jing Liang,[a] and Zhen-Yu Tian [a,*]

Received 00th January 20xx,
Accepted 00th January 20xx

DOI: 10.1039/x0xx00000x

www.rsc.org/

Cobalt oxide thin films were systematically synthesized on an inert carrier by pulsed-spray evaporation chemical vapor deposition (PSE-CVD). The effect of substrate temperature on the structure, morphology and surface composition of the prepared films was investigated by XRD, FTIR, SEM and XPS spectroscopies. An in situ diffuse reflectance infrared Fourier transform spectroscopy (In situ DRIFTS) and a gas chromatograph (GC) were involved to identify the surface and gaseous species occurred in the total oxidation of propene as a representative of VOCs, respectively. The structural analysis indicated that the obtained thin films transformed from CoO to pure Co_3O_4 spinel as the temperature raised from 350 to 450 °C. A homogeneous grain distribution was observed. For all samples, oxygen was mainly composed of lattice oxygen and adsorbed oxygen owned a minor proportion. The catalytic tests showed that all the thin films exhibited competitive performances to those of noble metals. According to the observed adsorption peaks of propene at low-temperature and transformation of CoO-Co_3O_4 from the in situ DRIFTS spectra, a combined redox and L-H mechanism was proposed for the catalytic oxidation of propene over cobalt oxide films. Porous structure and adsorbed oxygen on the film surface may well contribute to the catalytic oxidation of propene.

Introduction

Volatile organic compounds (VOCs) are one of the main air pollutants originated mainly from transportation and the combustion of different fuels.[1-3] Due to their toxicity to human health[4] and involvement in the formation of photochemical smog,[5] many countries have imposed restrict standards to reduce the industrial VOCs emissions. Several methods have been used in the past decades, such as thermal incineration,[6] biodegradation,[7] high-energy electron beam treatment,[8] adsorption[9] and absorption.[10] Recently, catalytic oxidation has attracted much attention as one of the most promising VOCs abatement technologies regarding its high efficiency and selectivity to CO_2.[11-14] Among the reported catalysts, transition metal oxides (TMOs) exhibit great potential due to its low cost and efficiency compared to the traditional noble metal catalysts.[15, 16] Specifically, cobalt oxides (CoO_X) show interesting catalytic properties for the deep oxidation of VOCs. A lot of works have been contributed to the synthesis, characterization and catalytic application of Co_3O_4[17-19] and cobalt-based oxides.[20-23] However, besides Co_3O_4 spinel, other cobalt oxides which contain low-valence cobalt are also expected to have promising catalytic activity. Although there are some works focusing on the preparation of individual Co_3O_4[18, 24-27] or CoO[28, 29] available, the systematic and controllable synthesis of CoO_X by a direct method for catalytic applications still remains a challenging task. Moreover, in many of the above-mentioned studies,[18, 27, 28] the substrates or supports generally play significant roles, which prevents the real evaluation of the catalytic performance of CoO_X. Thus, it is desired to prepare CoO_X on inert substrates.

CoO_X can be synthesized through several methods, including pulsed laser deposition (Co_3O_4),[18] sol–gel (Co_3O_4),[24] spray pyrolysis (Co_3O_4),[25, 27] sputtering (Co_3O_4),[26] electrodeposition (CoO),[28] hydrolysis (CoO),[29] solvothermal (Co_3O_4 and CoO)[30] and excess impregnation (Co_XO_Y).[31] However, with these methods, the purity of the acquired samples was usually difficult to ensure and some of them involved strict conditions or complex treatments. Compared to the above-mentioned techniques, pulsed-spray evaporation chemical vapor deposition (PSE-CVD) is easy to control the quality and thickness of the films on flexable substrates with low cost. In recent years, PSE-CVD has been applied widely to the synthesis of TMOs, such as Co_3O_4,[32] Mn_3O_4,[33] $Co_{3-x}Fe_xO_4$[34] and $Co_{3-x}Cr_xO_4$.[35] It should be mentioned that as a flexable substrate the satinless steel gird mesh is proved to have no or negligible catalytic effect and can be used for most reactors shapes. Thus, PSE-CVD exhibits great potential to preapre CoO_X thin films on satinless steel gird mesh for real evaluation of the catalytic performance of CoO_X samples.

The present work is oriented to synthsize the thin films of CoO_X by PSE-CVD in a tailored way. The effect of substrate temperature on the phases of the films was investigated. Several dedicated techniques were used to characterize the prepared films with respect to structure, chemical composition and morphological properties. The catalytic performance of

[a] Institute of Engineering Thermophysics, Chinese Academy of Sciences, 11 Beisihuanxi Road, Beijing 100190, China.
[b] University of Chinese Academy of Sciences, Beijing 100049, China.

†Electronic Supplementary Information (ESI) available: Experimental conditions; Results of repeated catalytic tests with coated nesh, NCM and a blank system; Standard IR spectrum for C_3H_6; In situ DRIFTS spectra for Mesh 350 and 450. See DOI: 10.1039/x0xx00000x

the grown CoO_X was investigated for the total oxidation of propene as a representative of VOCs in a fixed-bed quartz reactor. Furthermore, to get an insight into the catalytic mechanism, a newly developed in situ diffuse reflectance infrared Fourier transform spectroscopy (DRIFTS) was employed. With this setup, surface absorbed species can be detected during the catalytic test which provides information to understand the catalytic mechanism.

Results and discussion

Structure

The XRD patterns of the CoO_X thin films prepared at temperature range of 350–450 °C are displayed in Fig. 1. With the substrate temperature increasing from 350 to 450 °C, the obtained oxide transformed from CoO to pure Co_3O_4 gradually. For Mesh 350, peaks at 36.50°, 42.40°, 61.52° and 73.70° can be seen clearly, which are attributed to (111), (200), (220) and (311) orientations of CoO (JCPDS No. 43-1004), respectively. For Mesh 450, well-defined diffraction peaks are observed at 2θ of 19.00°, 31.27°, 36.85°, 38.54°, 44.81°, 55.66°, 59.36° and 65.24°, which correspond to (111), (220), (311), (222), (400), (422), (511) and (440) orientations of Co_3O_4 (JCPDS No. 42-1467). No characteristic peaks of any other impurities were observed with Mesh 450, revealing the high purity of the synthesized thin films. For Mesh 400, both the peaks of CoO and Co_3O_4 were observed, which indicates the formation of a mixture of CoO and Co_3O_4 spinel. Though weak peaks at 31.27° and 65.24°can also be observed for Mesh 350, the three main peaks manifest that the main composition of Mesh 350 is CoO. The crystallite sizes of the CoO_X oxides were estimated to be 20±5 nm by applying Scherrer's formula $D = 0.89\,\lambda/\beta\cos\vartheta$ to the most intense diffraction peak, where λ = 0.154056 nm and where β and ϑ represent the full width at half maximum (FWHM) and diffraction angle of the observed peak, respectively.[20]

In 2010, Heli and Yadegari reported the CoO preparation by using electrodeposition method.[28] Before deposition, their electrode needed special pretreatments such as polishing and sonication, and all solutions were prepared by doubly distilled water. However, their XRD results are too ambiguous to

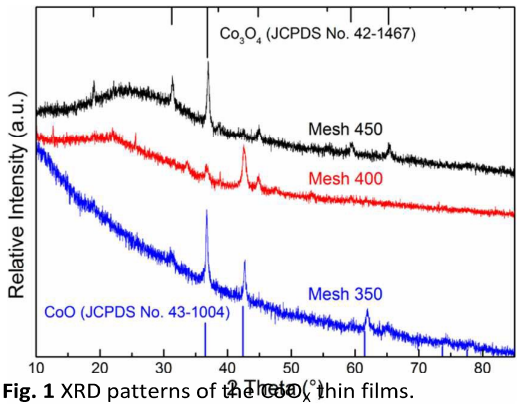

Fig. 1 XRD patterns of the CoO_X thin films.

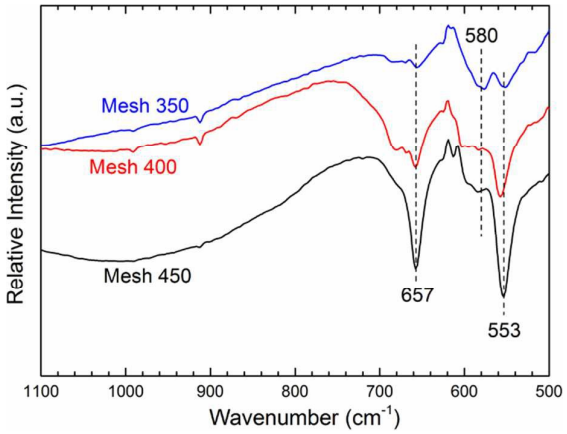

Fig. 2 Effect of the substrate temperature on the diffuse reflectance FTIR spectra of the prepared samples.

indicate the formation of pure CoO with good crystallization. Also, a large grain size (800 nm) was reported. Recently, Edla et al.[18] synthesized Co_3O_4 nanoparticles (NPs) by pulsed laser deposition. These NPs needed heating in Ar atmosphere to remove possible moisture adsorption before CO oxidation tests. The sizes of Co_3O_4 NPs were in the range of 18~500 nm which increased with the increasing laser fluence. These reported large grain sizes are expected to offer less surface area and thus lead to limited catalytic activity.

Further analysis with FTIR spectroscopy also confirmed the transformation of the phases from CoO to pure Co_3O_4 spinel. As presented in Fig. 2, two obvious bands with maxima at about 657 and 553 cm^{-1} can be observed and become stronger from Mesh 350 to Mesh 450. It should be noted that there is a strong peak at 580 cm^{-1} for Mesh 350, while such peak becomes weak for Mesh 400 and can be hardly recognized for Mesh 450 in view of relative intensity. According to the literature,[36, 37] the absorption peaks at 553 and 657 cm^{-1} are assigned to the transversal optical mode (TO) of Co_3O_4 and the peak at 580 cm^{-1} is due to the longitudinal optical mode (LO) of CoO. Therefore, from Fig. 2, it can be deduced that a pure Co_3O_4 was acquired at 450 °C and the sample prepared at 400 °C was a mixture of CoO and Co_3O_4, as for Mesh 350, CoO was the main composition synthesized at this temperature. Since exposure to the atmosphere, there are more Co^{3+} on the surface than the bulk average which will strengthen Co_3O_4 peaks in FTIR. So stronger peaks of Co_3O_4 were observed in Fig. 2 for Mesh 350 than Fig. 1.

Morphology

To have an insight into the surface morphology and spatial organization of the obtained CoO_X thin films, SEM was employed here. As displayed in Fig. 3, the morphology of the deposited thin films could also differ with substrate temperatures. For the sample prepared at 350 °C (Fig. 3a), highly dispersed tiny rods are distributed in the smooth amorphous oxide matrix, which is the highly agglomeration of these rods. Figure 3b shows a loose spatial organization and a blocky structure with amount of tiny folds. Especially, In

fact,beneath these large grains appeared at the surface, agglomeration of smaller structures can also be recognized. Since the grain sizes calculated by XRD data are smaller, it can be deduced that these large grains maybe supported by numerous tiny structures. As for the Co3O4 spinel obtained at 450 °C (Fig. 3c), numerous small grains with general agglomeration were observed. The micromorphology can be explained by the growth processes which contains nucleation, growth and coalescence process. For the initial grown grains, they could get a bigger size by further deposition and get close to each other. Then, by the coalescence of small ones the larger grains would appear. This agglomeration phenomenon was also observed in the pulsed laser deposition of Co3O4.18 From the three micrographs in Fig. 3, nano-structured particles were observed, which could be due to the agglomeration phenomenon. The size of these particles on the surface seems to be 30-40 nm on average, a little bigger than the values calculated by the XRD analysis. Barreca et al.38 had employed cold-wall low-pressure CVD to prepare CoOX previously, but the substrate needed sputtering as pretreatment. Rounded grains with diameter in the range of 340-580 nm were obtained.38 Spray pyrolysis had also been used to synthesize Co3O4 and got some overgrown clusters with the average size of 80 nm.27 Compared to these large grains, CoOX with much smaller grain size was obtained in the present work. Moreover, the tiny structure and loose spatial organization which always accompanied with a high specific surface area are expected to be beneficial to the catalytic performances.

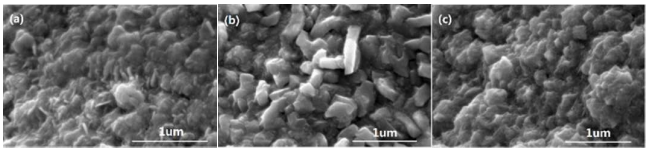

Fig. 3 SEM images of CoO_X thin films coated on stainless steel mesh; (a) Mesh 350, (b) Mesh 400 and (c) Mesh 450.

Chemical composition

To explore the chemical composition of the prepared thin films on stainless steel, XPS was carried out on both bare and etched surfaces of the CoO_X films. As depicted in Fig. 4, on the bare surfaces, much carbon was detected, which may be contamination products originated from precursor decomposition and ambient air. After 50 nm etching, carbon contamination is negligible. Figures 5 and 6 are the Co 2p and O 1s spectra after etching, respectively. To avoid Auger correction effect, only the Co $2p_{1/2}$ spectra were fitted. According to Gautier et al.,[39] the Co $2p_{1/2}$ peaks at around 795.0 eV are composed of Co^{2+} (796.4 eV) and Co^{3+} (795.2 eV). As shown in Fig. 5, all the samples are composed of Co^{2+} and Co^{3+}. The fitted results are in Table 1, Mesh 350 contains 91% of Co^{2+} and the calculated formula is $CoO_{1.05}$ which indicates that the main composition of Mesh 350 is CoO. Mesh 400 has a similar amount of Co^{2+} and Co^{3+} and the stoichiometric formula is $CoO_{1.29}$. For Mesh 450, the ratio of Co/O is 3:4.11, which is very close to Co_3O_4. These observations further

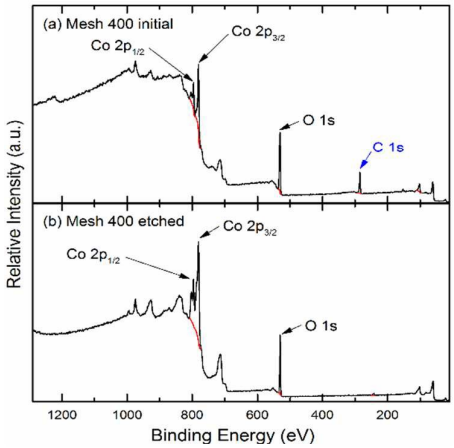

Fig. 4 Entire XPS spectra of Mesh 400 before (a) and after etching (b).

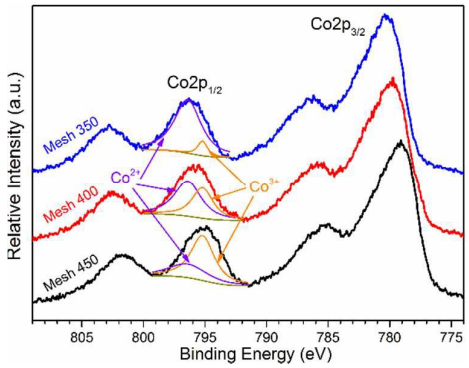

Fig. 5 XPS of Co 2p of the prepared CoO_X samples.

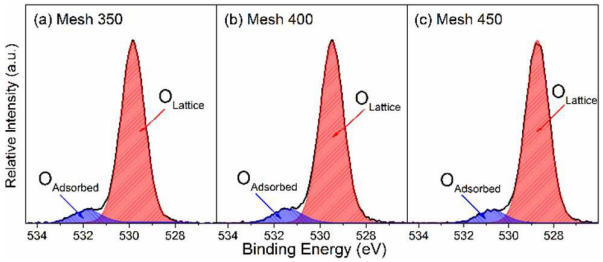

Fig. 6 O 1s signals of CoO_X thin films.

confirm the transformation of CoO to pure Co_3O_4 as the temperature increases from 350 to 450 °C.

The O 1s spectra of the synthesized films were deconvoluted into two peaks in the binding energy (BE) range of 528–532 eV in Fig. 6. The lower peak is attributed to the lattice oxygen species O^{2-}, and the other one is assigned to adsorbed oxygen.[40, 41] As depicted in the fitted O 1s spectra, all the samples were composed of two kinds of oxygen. In each sample, the atomic percentage of lattice oxygen was more than 90% and Mesh 400 possesses the most adsorbed oxygen (see Table 1). It is generally recognized that with TMOs catalysts, the lattice oxygen plays an important role in the

Table 1 Results of fitted Co $2p_{1/2}$ and O 1s of different samples

	Proportion	Stoichiometric formula	Atomic percentage (%)	
Sample	Co^{3+}:Co^{2+}	CoO_X	$O_{Lattice}$	$O_{Adsorbed}$
Mesh 350	0.09:0.91	$CoO_{1.05}$	92.1	7.9
Mesh 400	0.58:0.42	$CoO_{1.29}$	91.3	8.7
Mesh 450	0.74:0.26	$CoO_{1.37}$	92.7	7.3

catalytic oxidation process according to the redox mechanism. However, among the three samples, the amount of lattice oxygen has no much differences. Different amount of adsorbed oxygen may lead to differential catalytic performances since adsorbed oxygen may create more active sites for catalytic reactions.

Catalytic performance

Figure 7 compares the outlet profiles of C_3H_6, CO and C_2H_4 in the oxidation of C_3H_6 over three CoO_X samples and with NCM as reference. For the three coated meshes, the conversion of C_3H_6 becomes measurable at around 200 °C and complete conversion is reached within 400 °C. Mesh 350 and 400 exhibit slight better performance than Mesh 450 for about 25 °C with the complete conversion temperature. For the reaction with NCM, the consumption of C_3H_6 was found to be negligible up to 500 °C and 700 °C was needed to attain its complete conversion to CO_2. Table 2 summarizes the comparison of the catalytic performance of different catalysts by T_{90}. It is obvious that CoO_X samples prepared in this work are quite competitive to many other TMOs and noble metal catalysts. It is worth mentioning that these catalytic tests were repeated three times with the same sample and the results have no apparent difference (see Fig. ESI S1), demonstrating that the prepared CoO_X has good reusability.

The investigation of C_3H_6 oxidation over NCM showed no significant difference compared with a blank system (see Fig. ESI S2), suggesting that the mesh has a negligible catalytic effect and can be used as an inert carrier for the objective evaluation of deposited catalyst. In each case, CO_2 was observed to be the final product. CO and C_2H_4 were detected during the reaction process over NCM with a considerable amount which can be attributed to the partial oxidation. In contrast, no traces of CO or C_2H_4 were detected with any coated meshes, as indicated in Fig. 7b (Mesh 350 and Mesh 450 have overlapped with Mesh 400, so only Mesh 400 was given as a representative), demonstrating that CoO_X is an effective catalyst for the C_3H_6 oxidation at low temperatures.

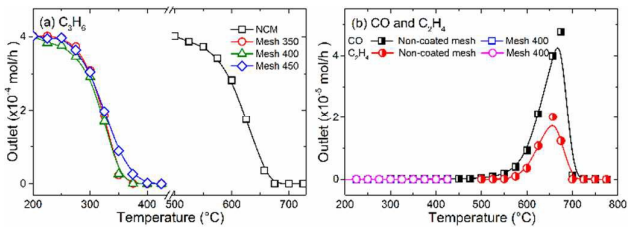

Fig. 7 Outlet profiles of C_3H_6 (a), CO and C_2H_4 (b).

With an Arrhenius expression for evaluation of the light-off profiles in the region where less than 15% of C_3H_6 was converted, apparent activation energies (E_{appa}) were calculated following reference.[17] Figure 8 compares the E_{appa} values obtained in this work. The reaction with Mesh 400 shows relatively low E_{appa} (78.1 kJ/mol) which indicates its high reactivity at low temperatures. It increases to 107.1 and 132.6 kJ/mol with Mesh 450 and 350, respectively. The non-catalyzed reaction presents an E_{appa} of 95.8 kJ/mol which is surprisingly lower than Mesh 350 and 450. Above all, E_{appa} is a parameter which focuses only on the initiation of the chemical reactions. Only with a low E_{appa} does not mean high-activity and can't promise a low temperature for complete conversion of the fuel molecules. The results indicate that the activity of catalysts increased greatly as temperature increases while NCM exhibits inert activity. For the initiation processes of propene oxidation, crystal defects formed in the preparation of Mesh 350 and 450 samples could make them less active. On the other hand, the oxygen vacant sites, which normally play key roles in the redox mehcanism, tend to increase from 350 to 400 °C and then decrease from 400 to 450 °C, enabling Mesh 350 and 450 to exhibit high E_{appa} values. This is supported by the lowest E_{appa} and best performance for sample Mesh 400. Moreover, the adsorbed oxygen on the NCM could benefit for the initiation of propene oxidation, which leads to a low E_{appa} with NCM. Compared with Mesh 350 and Mesh 450, Mesh 400 have a loose spatial organization and so higher specific surface area to absorb more oxygen and fuel, this behavior may promote the activation process. Moreover, from XPS results, Mesh 400 owns the most adsorbed oxygen, which can provide more active sites in the catalytic process. For Mesh 350, though with a higher E_{appa}, the complete conversion temperature is lower than Mesh 450 by 25 °C, which can be due to its higher mobility of lattice oxygen according to its better reducibility with more Co^{2+}.[42]

Mechanism

In order to reveal the possible catalytic mechanism over the prepared CoO_X, in situ DRIFTS was performed. To identify the characteristic peaks of C_3H_6, pure gas of C_3H_6 was measured first using an IR chamber and the observed spectrum is showed in Fig. ESI S3. For this in situ DRIFTS test,

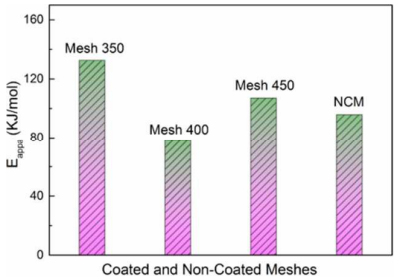

Fig. 8 The apparent activation energy (E_{appa}) of NCM and coated meshes prepared at 350, 400 and 450 °C during catalytic processes of C_3H_6.

Table 2 Comparison of T_{90} of different catalysts

Catalyst	Weight (mg)	Inlet composition	Flow rate (ml·min^{-1})	T_{90} [a] (°C)	Ref.
Mesh 350	13	1% C_3H_6/ 10% O_2 in Ar	15	347	This work
Mesh 400	13	1% C_3H_6/ 10% O_2 in Ar	15	348	This work
Mesh 450	13	1% C_3H_6/ 10% O_2 in Ar	15	369	This work
Co_3O_4	12	1% C_3H_6/ 10% O_2 in Ar	15	380	[32]
Co_3O_4	12	2% C_3H_6/ 20%O_2 in Ar	15	385	[43]
Co_3O_4	41.5	0.4% C_3H_6/ 3.6%O_2 in Ar	500	356	[17]
$Co_{2.66}Mn_{0.34}O_4$	12	2% C_3H_6/ 20%O_2 in Ar	15	356	[43]
CuO	12	1% C_3H_6/ 10% O_2 in Ar	15	301	[44]
Cu_2O	20	1% C_3H_6/ 10% O_2 in Ar	15	375	[45]
Mn_3O_4	12	1% C_3H_6/ 10% O_2 in Ar	15	403	[33]
$Co_{2.1}Fe_{0.9}O_4$	20	1% C_3H_6/ 10% O_2 in Ar	15	382	[46]
$CuCo_2O_4$	12	1% C_3H_6/ 10% O_2 in Ar	15	384	[47]
$La_{1.7}Sr_{0.3}CuO_4S_{0.2}$	200	0.1%C_3H_6/ 5% O_2 in N_2	100	500	[48]
$Co_{0.3}Ce_3O_{6.4}$	200	0.1% C_3H_6/ 9% O_2 in He	120	351	[49]
Au/Al_2O_3	4/200	0.15% C_3H_6/ 4% O_2 in He	75	410	[50]
Au/Al_2O_3	8.2/200	0.4% C_3H_6/ 3.6% O_2 in He	30	412	[51]
NCM	—	1% C_3H_6/ 10% O_2 in Ar	15	648	This work

Note: [a] T_{90} refers to the temperature at which 90% of the fuel is converted.

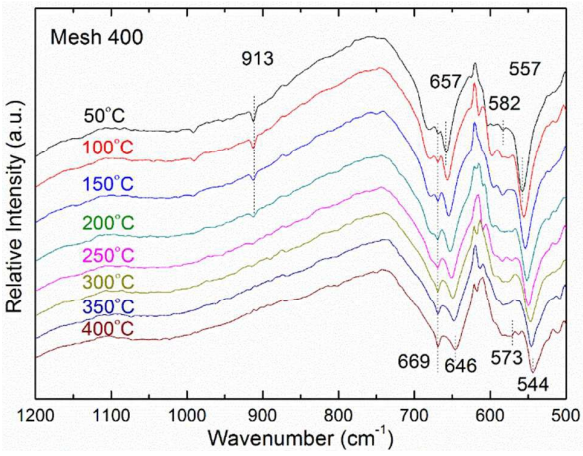

Fig. 9 In situ DRIFTS spectra of CoO_X prepared at 400 °C during C_3H_6 oxidation at different temperatures.

the spectra with Mesh 400 are presented in Fig. 9 as a representative and the left two spectra of Mesh 350 and 450 could be found in Figs. ESI S4 and S5, respectively. Figure 9 depicts the IR spectra at different temperatures. Among these absorption peaks, 913 cm^{-1} is assigned to the CH_2 wagging vibration of adsorbed C_3H_6 on the deposited film;[52] 669 cm^{-1} comes from the bending vibration of CO_2; 557 and 657 cm^{-1} are characteristic absorption peaks of Co_3O_4 and 582 cm^{-1} is attributed to CoO as depicted in Fig. 2. As can be seen from Fig. 9, spectra measured below 200 °C had strong adsorption peak of C_3H_6 (913 cm^{-1}). With temperature increasing, adsorption peak of C_3H_6 vanishes gradually and the peak attribute to CO_2 (669 cm^{-1}) become stronger. This indicates that during the catalytic process, C_3H_6 is adsorbed on the surface of the CoO_X catalyst firstly, and then the reaction rate of adsorbed C_3H_6 is accelerated as temperature increases and more CO_2 is generated. With a higher C_3H_6 consumption rate and so CO_2 production rate, the adsorption peak of C_3H_6 becomes weaker and the peak of CO_2 becomes stronger. With

in situ DRIFTS spectra, adsorption of C_3H_6 on CoO_X thin films was observed, which suggests that the catalytic reaction of C_3H_6 on CoO_X is preceded with the Langmuir-Hinshelwood (L-H) mechanism.

Normally, redox mechanism is acceptted for the catalytic oxidation of light hydrocarbons over TMOs as the metal ions can be circulated by reduction to lower ionic states and recovery to higher ionic states via re-oxidization.[53-55] In this work, Co^{3+} and Co^{2+} in the CoO_X thin films could be reduced to Co^{2+} and Co by releasing active oxygen. As temperature increases, adsorbed C_3H_6 will react with trapped or released oxygen. Co^{2+} and Co can then be reoxidized to form CoO_X by the replenished oxygen in the gas phase.[56, 57] Moreover, the electrophilic oxidation involving chemisorbed species O_2^- and O^- will promote the total oxidation of C_3H_6 to CO_2 over Co_3O_4.[57] It's worth noting that the catalysts take part in the reaction during the propene oxidation process and the chemical composition of the active surface is always changing as a consequence of sustainable oxidation-reduction, but the compositions of the catalysts would keep the same before and after the catalytic reaction.[43] This phenomena were also confirmed by running the catalytic tests several times and the same results were botained. As displayed in Fig. 9, with temperature increased from 50 to 400 °C, the three CoO_X adsorption bands at 657, 582 and 557 cm^{-1} exhibit red shift of 11, 9 and 13 cm^{-1}, respectively. The red shift is due to the change of vibration energy level as the temperature increases, which further indicates that more bulk oxygen is activated. From the random changes of the relative intensity of CoO and Co_3O_4, a sustainable transformation process between Co^{3+} and Co^{2+} can be proposed, which supports the redox mechanism in the oxidation of C_3H_6 over CoO_X.

Experimental

Synthesis of CoO_x films

The CoO_X thin films were synthesized in a PSE-CVD system combined with cold-wall stagnation point-flow CVD reactor and waste collector. The experimental setup can be found in our previous work[45] and typical deposition conditions are shown in Table ESI S1, respectively. Cobalt acetylacetonate ($Co(acac)_2$) was dissolved in ethanol with a concentration of 2.5 mM as the feedstock. The frequency and width of the injector are 4 Hz and 1.2 ms. The liquid feedstock, with a feeding rate of 1.0 mL/min, was injected as a fine spray into a 30-cm long evaporation chamber kept at 220 °C. The resulting vapor was transported to the deposition chamber, with N_2/O_2 flow rates of 0.25/0.75 standard liter per minute (SLM), respectively. Flow rates of gases were controlled by MKS mass flow controllers. The total pressure in the reactor during deposition was kept at 3.0 kPa. To meet the requirements of different characterization techniques, the deposition was performed on several types of substrates without any treatments, including bare glass, stainless steel and mesh grid of stainless steel. Mesh 350, Mesh 400 and Mesh 450 are defined as the deposited films on relevant substrate at 350, 400 and 450 °C, respectively. The substrates were heated using a flat resistive heater by a heating controller (HT60, Horst). The waste vapor was collected by a liquid nitrogen trap and the rest gases were pumped away. The weight of the deposited films was determined gravimetrically by measuring the weight change of the substrates with a microbalance (Sartorius).

Characterization

The phases of the deposited films obtained at different substrate temperatures were identified by X-ray diffraction (XRD) using a Bruker D8 Focus equipped with a Cu Kα (λ = 0.154056 nm) radiation source and operated at 40 kV and 40 mA. By referring to the Joint Committee on Powder Diffraction Standards (JCPDS) database cards, the crystalline phases were identified. The morphology of the deposited films was examined using SEM (QUANTA FEG 250). The characteristic vibrations of the prepared thin film catalysts were ascertained using a diffuse reflectance infrared Fourier transform spectroscopy (DRIFTS, Bruker VERTEX 70) with the spectral resolution of 4 cm^{-1} in the range of 400-4000 cm^{-1}.

Catalytic test

Small unsaturated hydrocarbons, such as propene (C_3H_6), is an important class of VOCs and quite difficult to be oxidized. In this work, the catalytic behavior of CoO_X was investigated toward the oxidation of C_3H_6 at atmospheric pressure in a fixed-bed quartz reactor with 13 mg catalyst grown on meshes of stainless steel. To exclude the effect of background, a contrast test using mesh grid without any deposition was performed. The experimental setup can be found elsewhere[45] and only a brief description is given here. A feed mixture of 1 vol.% C_3H_6 and 10 vol.% O_2 in the balance of argon was introduced into a tubular reactor at a total flow rate of 15 mL/min, corresponding to weight hourly space velocity (WHSV) of about 69,000 ml/g_{cat}·h. The temperature of the reactor was raised with a ramp of 5 °C /min using a digital electrical furnace. The exhaust gases were analyzed using a gas chromatograph (Agilent, GC3000).

To explore the catalytic mechanism, in situ DRIFTS tests were carried out. The stainless steel mesh with deposition was placed in the temperature-controlled chamber. C_3H_6/O_2/Ar with the ratio of 1%/10%/89% and a total flow rate of 15 mL/min were introduced into the chamber. The temperature of the chamber was raised with a ramp of 5 °C /min from room temperature to 400 °C during the tests. The background spectrum was deducted by measuring the spectrum of a non-coated mesh (NCM) in the in situ chamber under the same gas inlet conditions. By online monitoring the transform of the characteristic bands of CoO_X and absorption of fuel gases, possible catalytic mechanism can be proposed.

Conclusions

The one-step PSE-CVD method was applied to prepare CoO_X thin films from $Co(acac)_2$ by adjusting the temperature from 350 to 450 °C. The obtained samples were characterized in

terms of structure, morphology, surface composition and catalytic properties with XRD, FTIR, SEM, XPS and in situ DRIFTS. Structure studies demonstrate that with an increase of substrate temperature from 350 to 450 °C, the obtained oxides varied from CoO to pure Co_3O_4 spinel gradually. Adsorption of oxygen species is more with Mesh 400 than 350 and 450 which may benefit the catalytic performances. Catalytic tests indicate that CoO_X exhibit a competitive catalytic activity compared to supported noble metals and many other TMOs in the deep oxidation of C_3H_6. Mesh 350 and 400 showed slightly better performance over Mesh 450 due to its more low-valence cobalt, porous structure and more adsorbed oxygen. With increasing temperature, adsorption peaks of C_3H_6 and CO_2 were detected and surface conversion of CoO-Co_3O_4 was also observed during in situ DRIFTS tests. These observations indicate that the catalytic reaction was preceded with redox and L-H mechanism.

Acknowledgements

ZYT thanks the financial support from the Recruitment Program of Global Youth Experts. The authors thank Dr. Jun-Jie Weng and Mr. Bing-Yin Wang for help discussions.

Notes and references

* *Corresponding author. Tel/Fax: +86-10 82543184, E-mail: tianzhenyu@iet.cn.*

1. J. J. Schauer, M. J. Kleeman, G. R. Cass and B. R. T. Simoneit, *Environ. Sci. Technol.*, 2001, **35**, 1716-1728.
2. C. J. Cai, F. H. Geng, X. X. Tie, Q. O. Yu and J. L. An, *Atmos. Environ.*, 2010, **44**, 5005-5014.
3. P. R. Veres, P. Faber, F. Drewnick, J. Lelieveld and J. Williams, *Atmos. Environ.*, 2013, **77**, 1052-1059.
4. S. Batterman, F. C. Su, S. Li, B. Mukherjee, C. R. Jia and H. E. I. H. R. Committee, *Res. rep. Health Eff. Inst.*, 2014, 3-63.
5. T. Y. Chang and M. J. Suzio, *J. Air & Waste Manage. Assoc.*, 1995, **45**, 20-28.
6. *US, EPA, Air pollution control technology fact sheet, EPA-452/F-03-022*.
7. G. Chen, K. A. Strevett and B. A. Vanegas, *Biodegradation*, 2001, **12**, 433-442.
8. W. J. Cooper, M. G. Nickelsen, R. V. Green and S. P. Mezyk, *Radiat Phys Chem*, 2002, **65**, 571-577.
9. A. M. Mastral, T. Garcia, M. S. Callén, J. M. López, M. V. Navarro, R. Murillo and J. Galbán, *Environ. Sci. Technol.*, 2002, **36**, 1821-1826.
10. H. L. Huang and W. M. Lee, *J Environ Eng*, 2002, **128**, 60-67.
11. E. N. Ndifor, T. Garcia, B. Solsona and S. H. Taylor, *Appl Catal B-Environ*, 2007, **76**, 248-256.
12. K. Everaert and J. Baeyens, *Journal of Hazardous Materials*, 2004, **109**, 113-139.
13. P. Papaefthimiou, T. Ioannides and X. E. Verykios, *Appl Catal B-Environ*, 1997, **13**, 175-184.
14. S. Minicò, S. Scirè, C. Crisafulli, R. Maggiore and S. Galvagno, *Appl Catal B-Environ*, 2000, **28**, 245-251.
15. Z. Gu and K. L. Hohn, *Ind. Eng. Chem. Res.*, 2004, **43**, 30-35.
16. L. F. Liotta, M. Ousmane, G. Di Carlo, G. Pantaleo, G. Deganello, A. Boreave and A. Giroir-Fendler, *Catal. lett.*, 2009, **127**, 270-276.
17. Z. Y. Tian, N. Bahlawane, F. Qi and K. Kohse-Höinghaus, *Catal Commun*, 2009, **11**, 118-122.
18. R. Edla, N. Patel, Z. El Koura, R. Fernandes, N. Bazzanella and A. Miotello, *Appl Surf Sci*, 2014, **302**, 105-108.
19. K. Shojaee, B. S. Haynes and A. Montoya, *Appl Surf Sci*, 2014, **316**, 355-365.
20. Z. Y. Tian, N. Bahlawane, V. Vannier and K. Kohse-Höinghaus, *Proc Combust Inst*, 2013, **34**, 2261-2268.
21. A. Goyal, S. Bansal, V. Kumar, J. Singh and S. Singhal, *Appl Surf Sci*, 2015, **324**, 877-889.
22. A. Jamal, M. M. Rahman, S. B. Khan, M. Faisal, K. Akhtar, M. A. Rub, A. M. Asiri and A. O. Al-Youbi, *Appl Surf Sci*, 2012, **261**, 52-58.
23. D. H. Shang, Q. Zhong and W. Cai, *Appl Surf Sci*, 2015, **325**, 211-216.
24. K. J. Kim and Y. R. Park, *Solid State Commun*, 2003, **127**, 25-28.
25. P. S. Patil, L. D. Kadam and C. D. Lokhande, *Thin Solid Films*, 1996, **272**, 29-32.
26. H. Yamamoto, S. Tanaka and K. Hirao, *J Appl Phys*, 2003, **93**, 4158-4162.
27. V. R. Shinde, S. B. Mahadik, T. P. Gujar and C. D. Lokhande, *Appl Surf Sci*, 2006, **252**, 7487-7492.
28. H. Heli and H. Yadegari, *Electrochimica Acta*, 2010, **55**, 2139-2148.
29. L. Poul, S. Ammar, N. Jouini, F. Fiévet and F. Villain, *Solid State Sci.*, 2001, **3**, 31-42.
30. K. Deori and S. Deka, *Cryst. Eng. Comm.*, 2013, **15**, 8465-8474.
31. G. L. Zhou, H. M. Xie, B. G. Gui, G. Z. Zhang and X. X. Zheng, *Catal Commun*, 2012, **19**, 42-45.
32. P. Mountapmbeme Kouotou, Z. Y. Tian, U. Mundloch, N. Bahlawane and K. Kohse-Höinghaus, *RSC Adv.*, 2012, **2**, 10809-10812.
33. Z. Y. Tian, P. Mountapmbeme Kouotou, N. Bahlawane and P. H. Tchoua Ngamou, *J Phys Chem C*, 2013, **117**, 6218-6224.
34. N. Bahlawane, P. H. Tchoua Ngamou, V. Vannier, T. Kottke, J. Heberle and K. Kohse-Höinghaus, *Phys. Chem. Chem. Phys.*, 2009, **11**, 9224-9232.
35. V. Vannier, M. Schenk, K. Kohse-Höinghaus and N. Bahlawane, *J. Mater. Sci.*, 2012, **47**, 1348-1353.
36. M. Lenglet, J. Lopitaux, L. Terrier, P. Chartier, J. F. Koenig, E. Nkeng and G. Poillerat, *J Phys Iv*, 1993, **3**, 477-483.
37. B. Lefez, P. Nkeng, J. Lopitaux and G. Poillerat, *Mater Res Bull*, 1996, **31**, 1263-1267.
38. D. Barreca, C. Massignan, S. Daolio, M. Fabrizio, C. Piccirillo, L. Armelao and E. Tondello, *Chem Mater*, 2001, **13**, 588-593.
39. J. L. Gautier, E. Rios, M. Gracia, J. F. Marco and J. R. Gancedo, *Thin Solid Films*, 1997, **311**, 51-57.
40. G. Tyuliev and S. Angelov, *Appl Surf Sci*, 1988, **32**, 381-391.
41. S. Valeri, A. Borghi, G. C. Gazzadi and A. di Bona, *Surf. sci.*, 1999, **423**, 346-356.
42. P. Mountapmbeme Kouotou, Z. Y. Tian, H. Vieker, A. Beyer, A. Golzhauser and K. Kohse-Höinghaus, *J Mater Chem A*, 2013, **1**, 10495-10504.
43. Z. Y. Tian, P. H. Tchoua Ngamou, V. Vannier, K. Kohse-Höinghaus and N. Bahlawane, *Appl Catal B-Environ*, 2012, **117–118**, 125-134.
44. Z. Y. Tian, H. J. Herrenbrück, P. Mountapmbeme Kouotou, H. Vieker, A. Beyer, A. Gölzhäuser and K. Kohse-Höinghaus, *Surf Coat Tech*, 2013, **230**, 33-38.

45. G. F. Pan, S. B. Fan, J. Liang, Y. X. Liu and Z. Y. Tian, *RSC Adv.*, 2015, **5**, 42477-42481.
46. Z. Y. Tian, P. Mountapmbeme Kouotou, A. El Kasmi, P. H. Tchoua Ngamou, K. Kohse-Höinghaus, H. Vieker, A. Beyer and A. Gölzhäuser, *Proc Combust Inst*, 2015, **35**, 2207-2214.
47. Z. Y. Tian, H. Vieker, P. Mountapmbeme Kouotou and A. Beyer, *Faraday discuss.*, 2015, **177**, 249-262.
48. M. Machida, K.-i. Ochiai, K. Ito and K. Ikeue, *J. Catal.*, 2006, **238**, 58-66.
49. L. F. Liotta, M. Ousmane, G. Di Carlo, G. Pantaleo, G. Deganello, G. Marcì, L. Retailleau and A. Giroir-Fendler, *Appl. Catal. A: Gen.*, 2008, **347**, 81-88.
50. S. Ivanova, C. Petit and V. Pitchon, *Gold Bull*, 2006, **39**, 3-8.
51. A. C. Gluhoi, N. Bogdanchikova and B. E. Nieuwenhuys, *J. Catal.*, 2005, **229**, 154-162.
52. P. R. Griffiths and J. A. De Haseth, *Fourier transform infrared spectrometry*, John Wiley & Sons, 2007.
53. M. Labanowska, *Chemphyschem*, 2001, **2**, 712-731.
54. I. Aso, M. Nakao, N. Yamazoe and T. Seiyama, *J. Catal.*, 1979, **57**, 287-295.
55. M. Konsolakis, M. Sgourakis and S. A. Carabineiro, *Appl Surf Sci*, 2015, **341**, 48-54.
56. D. Duprez, *Catal. today*, 2006, **112**, 17-22.
57. J. Haber and W. Turek, *J. Catal.*, 2000, **190**, 320-326.